

LASCO White-Light Observations of Eruptive Current Sheets Trailing CMEs

David F. Webb¹ · Angelos Vourlidas²

Received: 16 February 2016 / Accepted: 2 September 2016 / Published online: 28 October 2016
© Springer Science+Business Media Dordrecht 2016

Abstract Many models of eruptive flares or coronal mass ejections (CMEs) involve formation of a current sheet connecting the ejecting CME flux rope with a magnetic loop arcade. However, there is very limited observational information on the properties and evolution of these structures, hindering progress in understanding eruptive activity from the Sun. In white-light images, narrow coaxial rays trailing the outward-moving CME have been interpreted as current sheets. Here, we undertake the most comprehensive statistical study of CME-rays to date. We use SOHO/LASCO data, which have a higher cadence, larger field of view, and better sensitivity than any previous coronagraph. We compare our results to a previous study of *Solar Maximum Mission* (SMM) CMEs, in 1984–1989, having candidate magnetic disconnection features at the CME base, about half of which were followed by coaxial bright rays. We examine all LASCO CMEs during two periods of minimum and maximum activity in Solar Cycle 23, resulting in many more events, ~ 130 CME-rays, than during SMM. Important results include: The occurrence rate of the rays is $\sim 11\%$ of all CMEs during solar minimum, but decreases to $\sim 7\%$ at solar maximum; this is most likely related to the more complex coronal background. The rays appear on average 3–4 hours after the CME core, and are typically visible for three-fourths of a day. The mean observed current sheet length over the ray lifetime is $\sim 12 R_{\odot}$, with the longest current sheet of $18.5 R_{\odot}$. The mean CS growth rates are 188 km s^{-1} at minimum and 324 km s^{-1} at maximum. Outward-moving blobs within several rays, which are indicative of reconnection outflows, have average velocities of $\sim 350 \text{ km s}^{-1}$ with small positive accelerations. A pre-existing streamer is blown out in most of the CME-ray events, but half of these are observed to reform within ~ 1 day. The long lifetime and long lengths of the CME-rays challenge our current understanding of the evolution of the magnetic field in the aftermath of CMEs.

Keywords Sun: corona · Sun: coronal mass ejections · Magnetic reconnection

✉ D.F. Webb
david.webb@bc.edu

¹ ISR, Boston College, Chestnut Hill, MA 02459, USA

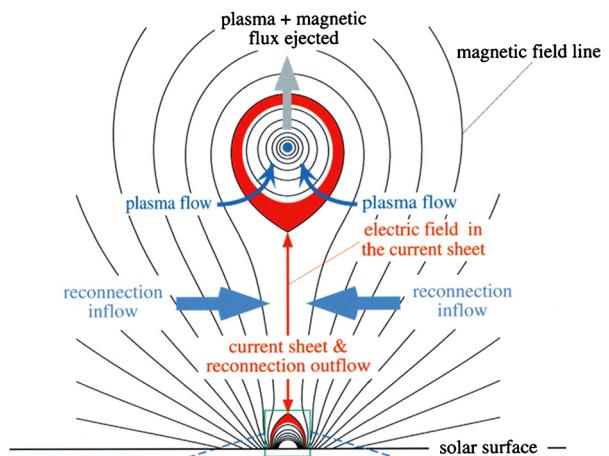
² Applied Physics Laboratory, The Johns Hopkins University, Laurel, MD 20723, USA

1. Introduction: Evidence of Reconnection and Current Sheets in the Corona

The disconnection of magnetic field lines following coronal mass ejections (CMEs) is an important aspect of a class of eruptive flare models, and some kind of reconnection appears necessary to prevent the buildup of the net interplanetary magnetic flux. Events showing evidence of disconnection have been detected in coronagraph data (*e.g.*, McComas, Gosling, and Phillips, 1992; Webb *et al.*, 2003) and *in-situ* as dropouts in the heat flux carried by beamed electrons (*e.g.*, McComas *et al.*, 1989). Such events have been observed both in isolation across streamers (*e.g.*, Wang *et al.*, 1999; DeForest, Howard, and McComas, 2012) and across the ray-current sheets trailing CMEs (this study). Although it is unclear how much each of these processes contributes to the net interplanetary magnetic flux balance, their importance to the evolution of the heliospheric current sheet (HCS) is apparent because streamers form the coronal base of the HCS, and CMEs frequently occur as the blowout of a streamer.

Models of eruptive flares or CMEs predict the formation of a current sheet (CS) beneath the erupting magnetic flux rope (*e.g.*, Lin and Forbes, 2000), as shown schematically in Figure 1. The so-called standard flare model has been developed and refined over the past several decades (*e.g.*, Svestka and Cliver, 1992; Shibata *et al.*, 1995; Lin and Forbes, 2000; Linker *et al.*, 2003; Lin, 2004; Chen, 2011). In this model a stressed magnetic arcade that may contain a core flux rope begins to rise. A CS with a strong guide field develops beneath it as external pressure causes oppositely directed magnetic field lines to converge and reconnect. The faster the eruption precedes, the higher the rate at which new field lines can accumulate at the CS. Some of the liberated energy heats and accelerates the CME plasma, adding mass and magnetic flux to it. Energy is also directed outward from the reconnection region as shock waves, energetic particles, and/or rapidly moving plasma. This energy can heat the low-lying or reconnecting magnetic loops and travel down the loops to the chromosphere, producing a two-ribbon flare. Thus, the CS forms and connects the outgoing CME and flux rope with the reforming coronal loop arcade near the surface (Figure 1). For many years, these were simply model predictions. We now have a growing body of evidence for the existence of such CSs in the corona trailing CMEs when the observing conditions are appropriate.

Figure 1 Schematic of the disrupted magnetic field that forms during a coronal mass ejection. Catastrophic loss of equilibrium, occurring in a magnetic configuration including a flux rope, stretches the closed field creating a Kopp–Pneuman-type structure. From Lin, Raymond, and van Ballegoijen (2004); reproduced by permission of the AAS.



Webb *et al.* (2003 – hereafter Paper 1) undertook a comprehensive study of white-light (WL) observations made by the NCAR High Altitude Observatory (HAO) *C/P coronagraph* (MacQueen *et al.*, 1980) on the field of view (FoV; $2\text{--}6 R_{\odot}$) of the *Solar Maximum Mission* (SMM) and the Mauna Loa Solar Observatory (MLSO) *K-coronameter* (Fisher *et al.*, 1981) in Hawaii (FoV: $1.2\text{--}2.2 R_{\odot}$) of transient rays that formed in the wake of CMEs, then faded or disappeared hours later. Webb *et al.* selected CMEs with a concave-outward (C-O) structure from the SMM CME catalog (Burkepile and St. Cyr, 1993), and called them Candidate Disconnection Events (CDEs). However, it is now commonly understood that such circular features are evidence of magnetic flux ropes within CMEs, viewed end-on (*e.g.*, Chen *et al.*, 1997; Dere *et al.*, 1999; Patsourakos, Vourlidis, and Stenborg, 2010; Vourlidis *et al.*, 2013). Paper 1 studied 59 of the CME/CDE events between June 1984 and mid-November 1989. The authors found that 58 % of the CME/CDEs, with adequate data coverage, were followed within about 12 hours by the transient rays that are suggestive of newly formed CSs. Paper 1 was the first to suggest that the post-CME WL rays were consistent with the existence of long-lived CSs extending $> 5 R_{\odot}$ into the outer corona. *We emphasize that in the present article, as in the previous WL ray studies, the CME-rays that are observed are considered proxies for CSs.*

With the advent of SOHO data in 1996, the studies of CSs in the corona increased significantly. In the LASCO (*Large-Area Spectroscopic Coronagraph* – Brueckner *et al.*, 1995) WL images, cases of CMEs with Y or C-O shapes and rays were reported by Simnett *et al.* (1997), and St. Cyr *et al.* (2000) found C-O features in about 40 % of all LASCO CMEs through June 1998. However, they did not examine the association of CME-rays with the C-O structures. Simnett (2004), Sheeley and Wang (2007), Vršnak *et al.* (2009), and Savage *et al.* (2010) identified bidirectional flows in SOHO and *Hinode* images moving away from a common point in the low to mid-corona that were interpreted in terms of reconnecting CSs. Ciaravella *et al.* (2002) provided spectroscopic evidence of the CME CS by showing that a narrow and hot region appeared between an outgoing CME and its associated flare arcade. This region was at the position where the CME arcade CS should be located. Bright narrow features with enhanced temperatures, densities, and abundances of elements with low first-ionization potentials were observed with the SOHO/*UltraViolet Coronagraph Spectrometer* (UVCS – Kohl *et al.*, 1995) following slow ($\sim 180 \text{ km s}^{-1}$; Ciaravella *et al.*, 2003) and very fast (1800 km s^{-1} ; Ko *et al.*, 2003; Lin *et al.*, 2005) CMEs. Lin *et al.* (2015) provided a recent comprehensive summary of observations related to eruptive current sheets.

Models such as those of Lin and Forbes (2000) imply that reconnection plasma flows should appear moving along the current sheet away from the diffusion region in opposite directions. The appearance of blobs of various sizes and speeds in a CME CS are very likely the result of different types of plasma instabilities and turbulence. Some laboratory results and numerical simulations such as reported by Riley *et al.* (2007), Shen, Lin, and Murphy (2011), Mei *et al.* (2012), and Guo, Bhattacharjee, and Huang (2013), which are summarized by Lin *et al.* (2015), can reproduce many of these observations. A long current sheet is particularly unstable to tearing mode turbulence. Thus, features such as a broadening of the reconnecting CS could be due to the combined effect of turbulence and development of slow-mode shocks.

Ko *et al.* (2003) studied the emission features and properties of a CS in detail, identifying plasma blobs flowing outward along the CS, and measured the speed of the reconnection outflow, the rate of magnetic reconnection, and the magnetic field strength near the CS. Lin *et al.* (2005) made direct measurements of the reconnection inflow speed near a CS, obtained the reconnection outflow speed of five moving plasma blobs, and the rate of reconnection.

Some of the rays in our study exhibited outflows and blobs, and we were able to make height–time measurements (see Section 3.7).

The analysis in Paper 1 was restricted in terms of data coverage and cadence, coronal FoV, and sensitivity. Since then, a large number of observational analyses of individual events and theoretical models and simulations have been published. Thus, now is the time to extend the statistical study of CME-rays or CSs to the more sensitive and extensive SOHO/LASCO coronagraph CME data set. In this article, we report results of a comprehensive examination of all LASCO CMEs in two periods during the minimum and maximum activity of solar cycle (SC) 23. *We emphasize that our focus is limited to the observational aspects of WL rays.* Recent articles such as that of Lin *et al.* (2015) provide reviews of comparisons of eruptive CS observations with models and simulations.

The article is organized as follows. In Section 2 we describe the LASCO CME observations of CME-rays and the construction of the CME-ray catalog. Section 3 provides the statistical results of the ray analysis in terms of occurrence rates, alignments and motions, durations or lifetimes, lengths, kinematics and widths, comparison of the basic parameters of the CMEs with rays vs. all CMEs, outflow or blob motions, and CME-streamer characteristics. In Section 4 we discuss the results, and we highlight the main conclusions in Section 5.

2. LASCO WL CME Observations and the CME-Ray Catalog

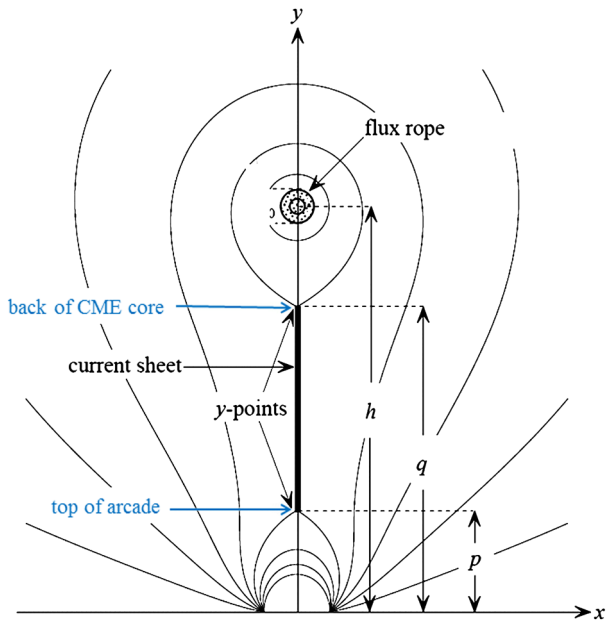
SOHO was launched in December 1995. LASCO is a suite of three coronagraphs. Currently, LASCO has two operating coronagraphs, C2, which images the middle corona from about 1.5 to 6 R_{\odot} , and C3, which overlaps with C2 and images the middle to outer corona, that is, about 3.5 to 32 R_{\odot} . The third LASCO coronagraph, C1, was an internally occulted narrow-band spectrometric instrument imaging the innermost corona, which was not recovered following the SOHO mission interruption in 1998.

As discussed by St. Cyr *et al.* (2000), the first LASCO observations used for CME statistical studies were obtained in January 1996, and synoptic cadences of images from both C2 and C3 began in early May 1996. Despite intermittent interruptions due to spacecraft and instrument anomalies and activities, an adequate duty cycle for CME detection was maintained until the unintentional loss of contact with the spacecraft in late June 1998. SOHO operations resumed in October 1998, and LASCO observations continue to the present.

Although LASCO has polarizing filters, nearly all of the LASCO CMEs have been identified in images obtained with the broad bandpass Orange (5400–6400 Å) filter. Before February 1997, the north and south polar regions of the C2 and C3 image frames were often truncated to conserve onboard computing and telemetry. LASCO was allocated additional telemetry after February 1997, providing more frequent C2 images and acquisition of full-frame images for both telescopes. LASCO has always been operated to emphasize synoptic observations, with a goal of about a one-hour cadence between C2 and C3 exposures. All but the very fastest CMEs are detectable with this cadence, with an overall LASCO duty cycle of 94 % (e.g., Vourlidas *et al.*, 2010, 2011). From early 1997 until 2010, C2 maintained a typical 24-min cadence and 40 min for C3. (The LASCO cadence was doubled in August 2010 when the SOHO mission transitioned to support the NASA LWS program.)

O.C. St. Cyr was the first Chief Observer for LASCO and developed the first LASCO CME catalog, in which he noted the occurrence of the C-O features with the CMEs. His catalog was maintained from January 1996 through to the end of June 1998 and is available online at ftp://lasco6.nascom.nasa.gov/pub/lasco/status/Version2_CME_Lists/. We used this

Figure 2 Modified diagram of the erupting flux rope model of Lin and Forbes (2000). The flux rope is driven upward because of a loss of equilibrium. Reconnection leads to a vertical current sheet, which, at any given time, extends from the Y-shaped points at the top of a growing arcade, $y = p$, to the base of the flux rope or back of the CME core, $y = q$. The heights and times of the leading edge of the CME (at top) and the Y points denoted by the blue arrows are measured for each event and appear in the CME-ray catalog (see Figure 3). The heights q and p are discussed in Section 3.4.



catalog to develop a new catalog of LASCO CMEs that had trailing coaxial rays, called the “SOHO/LASCO CME-Rays Catalog”. This catalog consists of serendipitous events identified from LASCO observations over many years, but incorporates a comprehensive survey of all LASCO C2 images for the period January 1996 through February 1998, which we define as solar minimum, and the entire year 2001, chosen as a typical activity maximum year for Cycle 23. This study is limited to these two periods, which are representative of the CME-rays during SC 23 sunspot minimum and maximum (see Figure 3). Note that the “minimum” includes an extended period of more than one year, which is necessary to achieve a statistically robust sample of CMEs and rays.

For our survey we viewed high-definition movies of the C2 images over five-day periods using the excellent SOHO Movie Theater hosted on the NASA SOHO site at http://sohodata.nascom.nasa.gov/cgi-bin/soho_movie_theater. We also used the direct and running-difference daily mpeg LASCO movies hosted by the NRL at http://lasco-www.nrl.navy.mil/daily_mpg/. Nearly all of the CMEs with rays that we identified are also listed in the CDAW LASCO CME catalog that is maintained by the NASA CDAW Data Center and The Catholic University of America (CUA) at http://cdaw.gsfc.nasa.gov/CME_list/index.html. We used this catalog for the basic measurements on each CME, such as first appearance time, central position angle (PA), angular width, speed, acceleration, mass, and kinetic energy.

Although LASCO permits viewing of structures out to the $32 R_{\odot}$ limit of C3, in this study the C2 data were primarily used for identifying the rays. The selection criteria for the events in the LASCO ray catalog were adapted from those used and described in Paper 1, as reviewed above, with one important difference. Paper 1 focused on (SMM) CMEs that were followed by an outward-moving structure, C-O or V- or U-shaped. This structure had to be morphologically connected to the CME and its front. These C-O features often occurred in the core region of the CME, which might consist of material associated with an erupting prominence. These CME core structures with adequate coverage were then searched for bright, narrow, linear, transient rays visually coaxial with the CME volume and appearing

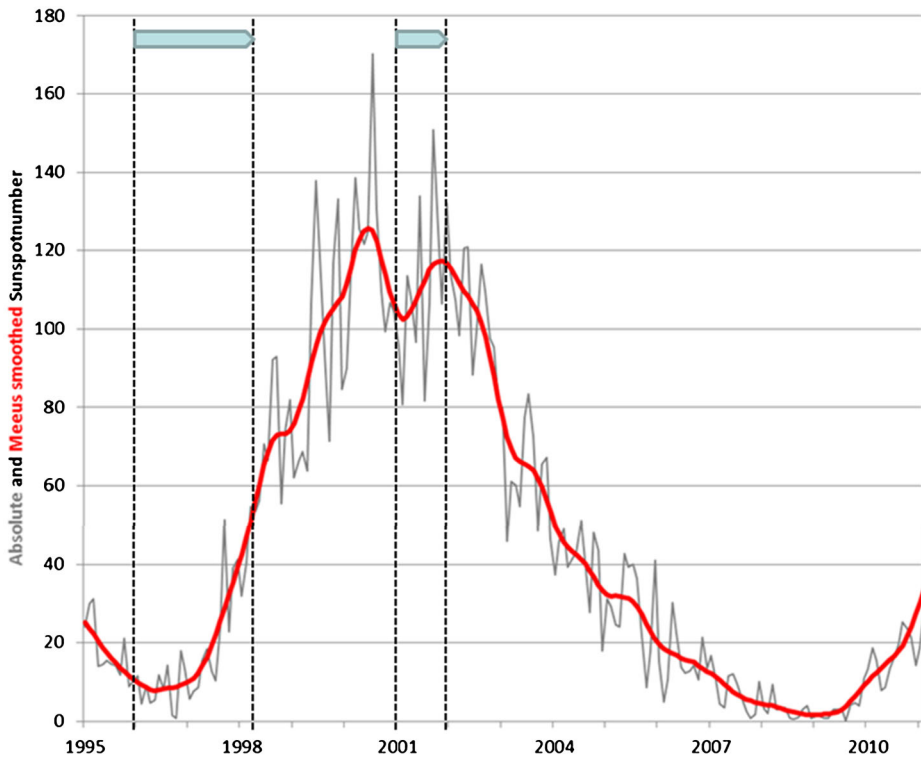


Figure 3 Plot of the monthly mean sunspot number (black line) for Solar Cycle 23, and the sunspot number smoothed with a Meeus smoothing function (red line). This function is similar to a 13-month box-car running average, but is tapered at the boundaries. The SC 23 minimum and maximum periods selected for our study are indicated between the vertical dashed lines. Courtesy F. Clette and WDC-SILSO, Royal Observatory of Belgium, March 2014.

within about 12 hours following CME onset. Thus, in the previous study the rays were a subset of the CMEs with C-O structures. In the current study, we examined *all* LASCO CMEs during two specific periods for the coaxial transient rays, regardless of whether the CMEs had C-O shaped cores. Once we identified a characteristic ray, we looked back and recorded whether the core was C-O. In nearly every case, the CME had a C-O core, which confirms the result of Paper 1.

For the LASCO study we required adequate data coverage during the candidate CME period, ideally for at least a full day starting from a few hours before CME onset. This allowed us to identify pre-existing structures, especially streamers, regardless of whether the streamer was blown out, whether a new streamer appeared in the wake of the CME, and any rays. For some long-duration CMEs and rays this required examination of the movies 3–4 days after CME onset.

The CME-ray measurements were keyed to the heights and times of the leading edge of the CME, the back of the CME core, or flux-rope region, and the top of the growing flare arcade. In the Lin and Forbes model these latter two points are schematically the upper and lower Y points that connect the current sheet (Figure 2). These measurements and their differences appear in the CME-rays catalog. A snapshot image of the first year of the catalog (without the comments) is shown in Figure 4. The catalog has columns for the CME location,

width, and speed (from the CDAW CME catalog), whether the CME core has a flux rope-like structure and, if so, what the best-observed time of the back of the core is, the ray onset time, whether UVCS [Fe XVIII] emission is observed (implying high plasma T), the ray duration, whether outflowing blobs move through the ray, whether there was a pre-existing streamer and if it was blown out by the CME, whether a new streamer later formed and the duration from CME onset to streamer formation, UVCS and MLSO data coverage, and comments. The complete catalog is available as an Excel file by contacting author David Webb.

The LASCO CME-rays catalog has been used in two recently published studies. In the first, Ciaravella *et al.* (2013) compared the LASCO ray list to UVCS CME data, primarily from a catalog (Giordano *et al.*, 2013, covering 1996–2005) linked to the CDAW LASCO CME catalog. In the ultraviolet spectra CSs are often identified as narrow bright features emitting in the [Fe XVIII] line. Ciaravella *et al.* (2013) analyzed samples of CME-rays or CSs detected in LASCO images or in ultraviolet spectra. Temperatures, widths, and line intensities of the rays were measured, and their correlation to the CME properties studied. The samples exhibited a wide range of temperatures. In some cases, the UV spectra supported the identification of WL rays as CSs, but in other cases the rays appeared to be cool material from the CME core.

In the second article, Ling *et al.* (2014) studied a bright ray trailing a very fast CME on 2005 September 7. MLSO Mk-4 polarized brightness images were used to study the initial stages of the formation and early development of the CME-ray or CS low in the corona. Coverage of the early development of the ray out to $\sim 1.3 R_{\odot}$ for a period of ~ 27 hr enabled a measurement of the CME-ray or CS from the top of the arcade to the base of the presumed flux rope. The kinematics of the upper and lower Y-points described in reconnection flux-rope models such as Lin and Forbes (2000) were used to determine the speed and acceleration of the growth of the ray or CS.

Figure 5 is a good example of the CME-rays that we studied. This was a fast (909 km s^{-1}), wide (125°), and bright streamer-blowout CME with a CME core followed ~ 3.5 hr later by a bright coaxial ray. This event was also a classic three-part CME with a bright front surrounding a void with an erupting prominence at its base. (An edge-enhanced version of this event is shown as Figure 1 in Ciaravella *et al.* (2013).) This event was a case where a new streamer appeared, or reformed, starting ~ 16.5 hr after CME onset.

3. Results

In this section we present the statistical results of the analysis of the LASCO CME-rays. These are discussed in the next subsections on occurrence rates, alignments and motions, durations or lifetimes, lengths, kinematics and widths, comparison of the basic parameters of the CMEs with rays *vs.* all CMEs, outflow or blob motions, and CME-streamer characteristics. The mean values for each of these categories are derived separately for the solar minimum and maximum periods and are compared (Tables 1–6). The equivalent results from Paper 1 for the SMM period 1984–1989 are listed in the last row of Tables 2–4 and 6.

3.1. Occurrence Rates

Paper 1 listed 124 definite or possible C-O CME cores observed over the 5.5-year period following the SMM repair, suggesting that about 10 % of all the SMM CMEs had C-O cores, in agreement with Webb and Cliver (1995). Paper 1 analyzed 59 of the best-observed

| SOHO LASCO CMEs-rays | | | | | | | | | | | | | | | | | | | | | | |
|---|-----------------------|-------------------|-----------------|-----------------|---------------------------|----------------------------------|----------------------------------|-------------|-----------------------------------|---------------------------------------|------------------------------------|----------------|--------------------|-----------------|------------------------------------|-----------|----------------|-----------------|--------------------|--------------------|-------------|----------|
| Webb, 2 Jan. 2015 | | | | | | | | | | | | | | | | | | | | | | |
| UVCS "no rays" removed | | | | | | | | | | | | | | | | | | | | | | |
| C2 | C2 | C2 | C2 | C2 | (Best) | Y-CME | Coastal | Ray-Y | Ray | CME-ray | Ray | Ray | Ray | | | | | | | | | |
| First Obs. U.T. | PA-Dir./Width [kmsec] | Speed-Acl [kmsec] | Mass [e+18 gr.] | K.E. [e+30ergs] | FFI C-O7 First Obs. (hrs) | (Best) FFI C-O7 First Obs. (hrs) | ray? UVCS First Obs. (hrs) | Ray-Y (hrs) | Ray PA(°) [dist. (Y) Motion Dir.] | CME-ray PA(°) [dist. (Y) Motion Dir.] | Ray Last Obs. (hrs) | Ray Dur. (hrs) | Moving Blobs (hrs) | Y speed [kmsec] | Y accel. [ms ⁻²] ratio | P-E Str ? | New Str ? | CME-Str (hours) | UVCS Data/ Feature | MK34 Data/ Feature | | |
| 1996 | 1996 | | | | | | | | | | | | | | | | | | | | | |
| 13-14 Jan. 22:08 | 267-VL 26 | 267-VL 229 | xxx | xxx | 14, 05:46 | 7:38 | Y-back of FR | 4:30 | 268 N-S? | 1 same | late in day | ~12 | N? | N | | Y-BO | N | xxx | NN | NN | BN,LY (Y/N) | |
| 15 Jan. 7:01 | 267-VL 56 | 467 | xxx | M | 10:55 | 3:54 | Y? 2 rays? | 2:43 | 268 No | 1 same | 2nd ray thru | >10 | N? | N | | N | DG, can't tell | xxx | NN | NN | YN? | |
| Synoptic evidence in C2 and C3 began early May 1996 | | | | | | | | | | | | | | | | | | | | | | |
| 11 May. 8:31 | 269-VL 54 | 165 | 0.49 | N? | xxx | xxx | Y-brief | xxx | 270 No | 2 same | ~20:00 | 5 | N? | N | | N | N? | xxx | NN | NN | YN? | |
| 8 July. 6:28 | 269-VL 40 | W/SW 476-N | 3.10 | Y | 13:13 | 6:45 | Y after 2 hr DG | <3:41 <3:68 | 280 No | 0 same | 20:00 | >3 | N? | 214 | 8.48 | Y? | can't tell | xxx | No VL d | No VL d | YN? | |
| 28-29 July ~18:00 | 267-VL 56 | 125-A | ? | ? | Y?-Vahpa | 5:20 | Y-back of FR | 0:00 | 262 No | 5 rays P | >23:05:54 | >7 | N | 110-270 | at 5-6 | Y | Y | >18:23 | No VL d | No VL d | YN | |
| 29-30 July ~17:06 | 265-VL 38 | W/SW 269-A | xxx | xxx | Y-sm. | 30, 00:30 | Y-back of FR, sharpens prev. ray | 2:24 | 265 No | 10 E | after midday broadens | ~12? | N | 202 | 0.04 | N | ? | xxx | YN | YN | YN/PN | |
| 22 Aug. 8:38 | 85-SE 110 | 717 | xxx | xxx | 9:09 | 0:27 | Y-back of FFI? p-e str | 0:48 | 119 No? | 34 P | Start next day blends when big str | >15 | N | 298(C3) | -4.8 | Y-BO | can't tell | xxx | YN | YN | N-22 | |
| 19-21 Oct. 2:39 | 130-SE 50 | 644-A 71-N | ? | ? | 16:35 | 13:56 | Y-not clear till later | 11:21 | 135 No? | 6 P | end 20th | ~20 | Y? | N | | Y-BO | N? | xxx | YM | YM | YN? | |
| 5-6 Nov. 2:35 | 274-VL 63 | 108-A | 0.27 | Y | ~16:11 | ~13:36 | Y maybe 2 | ~0 | 275 No | 1 same | 6, 02:35 | 11.5 | N | 54-310 | at 5-6 | ? | (fam) | Y | 22 | NN | NN | 5N,6Y-AN |

Figure 4 An image of the first page of the SOHO/LASCO CME-Rays Catalog. The values in red are derived quantities used in the analysis.

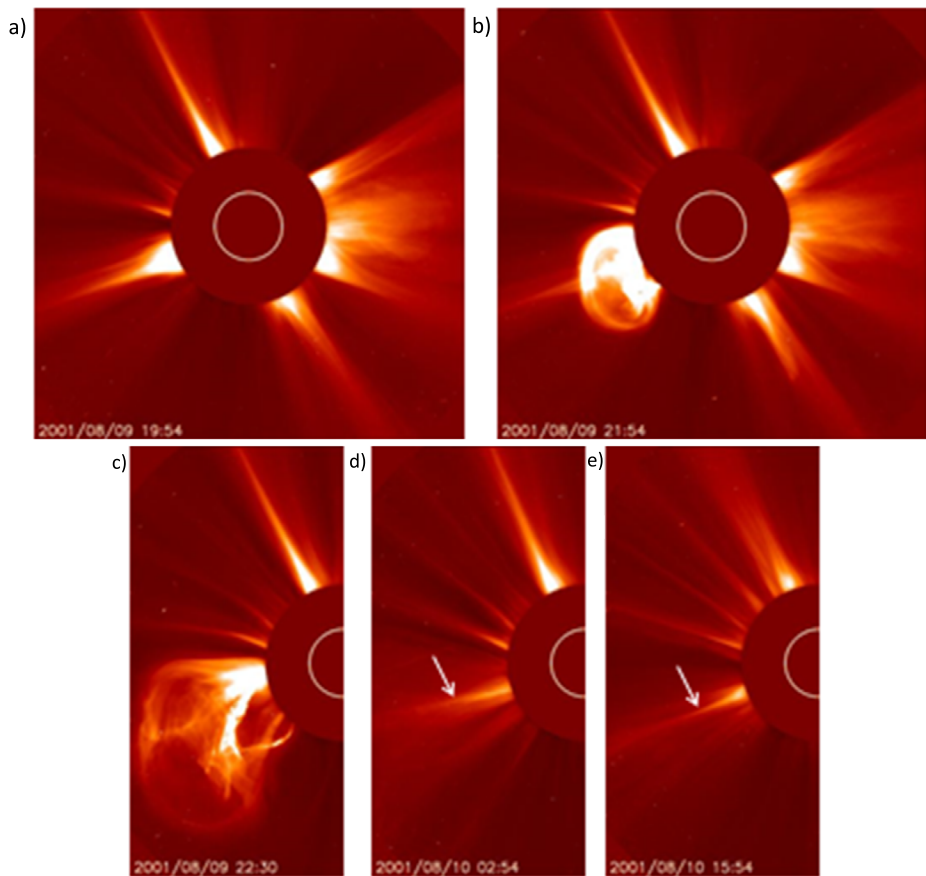


Figure 5 An example of a CME-ray event on 9–10 August 2001 in LASCO C2 images. This was a fast, wide, and bright streamer-blowout CME with a C-O core followed ~ 3.5 hr later by a bright coaxial ray. The sequence shows a) the swelling and brightening of the pre-existing streamer, b) its blowout as the fully formed CME, c) the CME with its C-O core and erupting prominence at the base, d) the later-forming ray (arrow), and e) the streamer reforming (arrow) ~ 19 hr after CME onset.

CME/C-O events, 58 % of which were followed within about 12 hours by the transient rays. This rate of SMM cores with rays implies that, averaged over the SMM period, ~ 6 % of all CMEs had associated transient rays.

In this study we began with St. Cyr's CME catalog over the period defined as cycle minimum, January 1996–February 1998. We first examined all of St. Cyr's CMEs for trailing transient rays, and then used this experience to perform a comprehensive search of the remaining LASCO CMEs, guided by the CDAW catalog that superseded St. Cyr's catalog. (Reconciliation of the two LASCO CME catalogs through June 1998 was discussed in Yashiro *et al.* (2004).)

Recently, Wang and Colaninno (2014) showed that due to a selection effect, eliminating so-called “very poor events” from the manual (CDAW) LASCO catalog results in lower CME rates since 2005 and an improved correlation with sunspot number. We suggest that eliminating narrow CMEs, that is, those with widths $< 20^\circ$, from the CDAW catalog, and those with fewer than four measurements has the same effect (see also Vourlidas *et al.*,

Table 1 Occurrence rates of LASCO CMEs with rays and all CMEs.

| 1 | 2 | 3 | 4 | 5 | 6 | 7 | 8 |
|----------------|----------------|-----------------------------|-------------------|------------------|----------------------------------|-------------------------|----------------------|
| Period (year) | All CME counts | CMEs $W > 20^\circ$ counts* | CMEs w/ray counts | Duty-cycle corr. | Corr. CMEs $W > 20^\circ$ counts | Corr. CMEs w/ray counts | % CMEs-rays/all CMEs |
| 1996–Feb. 1998 | 516 | 425 | 43 | 1.07 | 455 | 52 | 11.4 |
| 2001 | 1392 | 1183 | 86 | 1.05 | 1242 | 90 | 7.2 |

* All CMEs $> 20^\circ$ width, with measured masses and > 3 measurements (Vourlidas *et al.*, 2010, 2013).

Table 2 Summary of ray measurements.

| 1 | 2 | 3 | 4 | 5 | 6 | 7 | 8 |
|--------------------------|-----------------------------------|--------------------|-------------------|--------------------------------|--------------------------------|------------------------|--|
| Period (year) | Offset, CME-ray axes ($^\circ$) | Dir. of offset | Ray motion? | Duration; core–CME onsets (hr) | Duration; ray–core onsets (hr) | Ray lifetime (hr) | Highest C3 meas. (R_\odot) |
| 1996–Feb. 1998 | 6.2 (43); 0–34 | 12N, 18E, 13P (43) | 31N, 9Y, 1 ? (41) | 6.8 (38); 0–34.9 | 3.7 (39); 0–13.15 | 18.2 (25); 5–60 [10 >] | 11.8 (19); 7–17 |
| 2001 | 8.9 (79); 0–36 | 14N, 23E, 40P (77) | 78N, 6Y, 1 ? (85) | 3.0 (51); 0–12.6 | 3.2 (47); 0–17.7 [3 <] | 16.0 (57); 3–72 [20 >] | 12.4 (33); 8–18.5 |
| SMM; 1984–1989 (Paper 1) | 9.1 (27); 1–24 | 2N, 5E, 20P (27) | 13N, 10Y (23) | 7.9 (22); 1.5–15.3 | 3.8 (24); 0–10.5 | 7.8 (23); 1.5–23 [9 >] | [“Length”] > 11.3 (14); > 5.5 – > 21.4 |

2013). Although we visually examined all of the LASCO CMEs for this study, only the counts of CMEs with widths $> 20^\circ$ and with a measured mass and more than three measurements were used for the occurrence rate and basic CME statistics (Tables 1 and 4, respectively).

As shown in Table 1, we found 43 trailing rays during the minimum period. After eliminating the narrow CMEs (columns 3 and 6) and correcting for duty cycle (column 5), we found that 11.4 % of all LASCO CMEs during minimum had observable rays or CSs (Table 1, last column). When we extended this to the cycle maximum year 2001, 7.2 % of LASCO CMEs during maximum had rays or CSs. The SC 23 maximum rate agrees favorably with that found for the SMM period during SC 21/22 (Paper 1), but the minimum rate is higher. The lower occurrence rate during maximum is probably related to the reduced visibility of the rays, which is a result of the more complex corona and overlapping events.

3.2. Alignments and Motions of the Rays

Table 2 summarizes the statistical results for the alignments, motions, and lifetimes of the CMEs and their associated rays. Column 1 lists the time period, and column 2 lists the means, number of measurements in parentheses, and the range of values of the angular distance between the central axis of the CME and the ray. In a coronagraph image the CME central axis is generally the midpoint between the lowest and highest PAs of the measured CME width, essentially along the y-axis shown in Figure 2. We typically used the value listed in the CDAW CME catalog. For example, for “6.2 (43), 0–34” in the second column and second row, “6.2” specifies the mean value in degrees of the offset angle between the

CME central axis and the ray, “(43)” means a total of 43 measurements were made, and “0–34” is the range in degrees of the offset angles. Column 3 gives the direction of any offset, *i.e.*, whether the ray was coaligned with (N = null), equatorward (E) or poleward (P) of the CME axis. Thus in the third column and second row, “12N, 18E, 13P (43)” means that 12 events had rays exactly co-aligned with the CME axis, in 18 events the rays were equatorward of the CME axis, in 13 events the rays were poleward of the CME axis, and a total of 43 measurements were made. Column 4 lists whether the ray exhibited lateral motion during its lifetime. We estimate that our measurements are accurate to $\pm 1^\circ$. Columns 5–6 list the means of the timing data related to the lifetimes of the rays (column 7), and their highest measured heights (column 8), discussed in Sections 3.3 and 3.4, respectively.

The mean of the angular offset between the axes of the CMEs and their associated rays was $\sim 6^\circ$ ($\sim 9^\circ$) during minimum (maximum). This agrees with the SMM result of $\sim 9^\circ$ (Paper 1). At maximum most of the rays (52 %) lay poleward of the CME axis, similar to SMM (74 %). During minimum, however, it was mixed with only slightly more of the rays lying equatorward (42 %) of the CME axes. Most of the rays were coaxial with their accompanying concave-outward structure, but this is mostly a selection effect since the rays were required to be visually (*i.e.*, approximately) coaxial with their associated C-O structure.

In terms of lateral motion exhibited during the ray’s lifetime (column 4), most of the rays did not display any systematic motion. There was, however, a tendency for a higher fraction of moving rays to occur during minimum (9/41; 22 %) than during maximum (6/85; 7 %). This solar cycle-dependency of ray motions was similar to that found in Paper 1 for the SMM period: “most of the moving rays occurred during the minimum and rising phases of the cycle, 1984 through mid-1987, and most of the stationary rays were during the maximum phase from late 1988 through 1989.”

3.3. Durations or Lifetimes of the Rays

The last four columns of Table 2 summarize the statistical results of the timing, lifetimes, and heights of the rays. We use the time intervals between the appearances of certain features to estimate the durations or lifetimes of the features, in particular of the transient rays. We considered four time markers for each of the events. These are 1) the time of the C2 image on which the CME front was first detected; 2) the time of the image when the C-O core feature was first clearly visible; 3) the time of the image when the ray was first clearly visible; and 4) the time of the image when the ray was last clearly observed. In general, a feature’s “first-observed” or “last-observed” time means it was not seen on the previous or following C2 image, respectively. The C2 images were typically 24 min apart. The ray end time was the most difficult to quantify since the ray typically faded gradually into the background, or became a new streamer. These time markers (in UT) yield three time intervals or durations: 1) between the CME onset and the C-O core appearance, 2) between the C-O core appearance and the ray onset, and 3) between the ray onset and the ray end. The mean values of these are given in columns 5–7, respectively. The difference between the ray onset and ray end is defined as the ray “lifetime”, shown in column 7.

The mean interval between CME and core onset times (column 5) was 6.8 hr for minimum, more than twice that as during maximum, 3.0 hr. During minimum conditions CMEs tend to be weaker and slower than during maximum (see the next section). The mean SMM value was 7.9 hr, similar to the LASCO minimum interval.

Confirming the SMM result, the mean interval between the appearance of the C-O (core) feature and the ray onset (column 6) was 3.7 (3.2) hr for CME-rays during minimum (maximum). Thus, typically a ray brightened relatively quickly several hours after its apparent

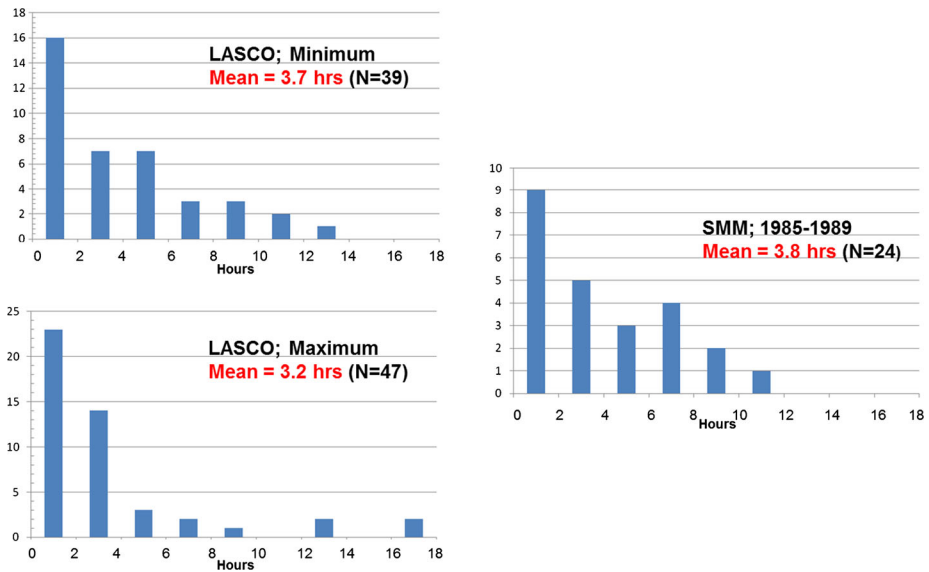


Figure 6 Histograms of the intervals in hours between the appearance of the C-O core and the ray onset. The time bins are each two hours. Rays can appear trailing from the CME core, or can appear suddenly hours later.

formation during eruption of the flux rope. Figure 6 shows histograms of these durations for the two LASCO intervals and the SMM results. The range of values is large, with some rays detected in the same image as the C-O core, especially when they were connected to the CME core. *This appearance or brightening delay of the current sheet is not understood (see Discussion).*

Column 7 of Table 2 gives the difference between the ray onset and ray end. This “lifetime” averaged 18.2 (16.0) hr during minimum (maximum). Some of these values are uncertain and reflect the difficulty of identifying a clear end time for fading rays and, thus, the values are likely lower limits. Histograms of the ray lifetimes for the two LASCO intervals and the SMM results are shown in Figure 7. Again there were large ranges in this value, and about one-third of the durations were lower limits. The LASCO results suggest that WL CME-rays are typically visible for more than half a day, significantly longer than their SMM lifetimes. This difference is most likely due to the much higher sensitivity of the LASCO images, the higher signal-to-noise ratio between ray and coronal background, and the larger FoV.

3.4. Height or Lengths of the Rays

Figure 8a is an example plot of height–time measurements of the trailing edge of a CME through the FoVs of both C2 and C3. These measurements tracked the C-O edge of the core closest to the Sun and along the CME axis-ray radial. The goal was to track the upper Y-point of the CS, or the distance q to the base of the flux rope in the model of Lin and Forbes (Figure 2). The line is the linear fit, and the scatter of the points about that line is an indication of the accuracy of the measurements. As expected, this scatter is greater above $4 R_{\odot}$. The best-fit line yields the velocity, shown in the figure.

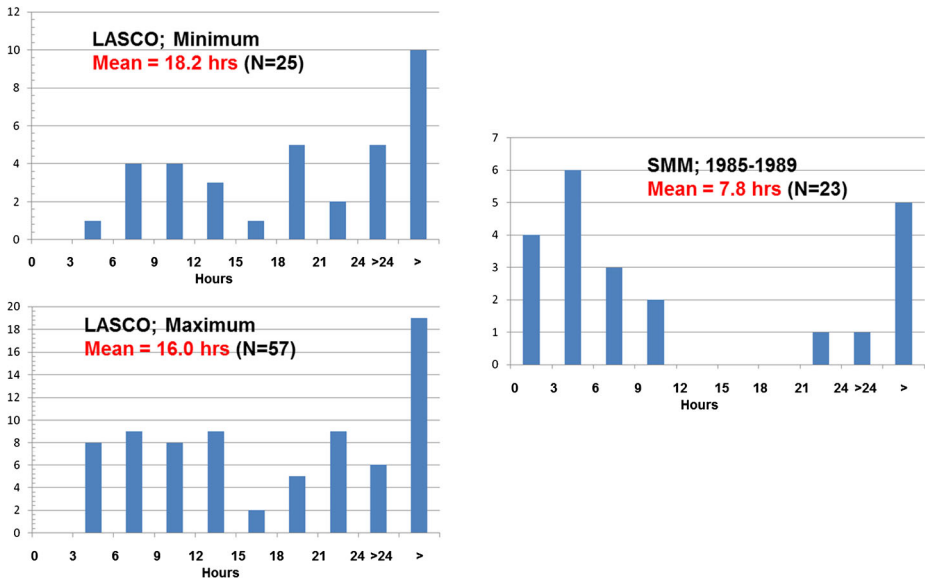


Figure 7 Histograms of the time differences in hours between the ray onset and ray end, which is defined as the ray “lifetime”. The time bins are each two hours. The ray lifetimes average ~ 3/4 day. One-third of the durations are lower limits, as indicated in the “>” values on the right side of each panel.

A clear and still unique feature of LASCO is that we can observe structures in the corona as far out as the outer edge, ~ 30 R_{\odot} , of the C3 FoV. We suggest that height–time measurements of the back of the core feature in the C3 FoV, such as in Figure 8a, provide a new way of directly measuring the length of current sheets in WL. For example, the highest point at which a good measurement of the core in this event could be made was 10.5 R_{\odot} . The mean of all such “final” heights measured in the C3 FoV is given in column 8 of Table 2: 11.8 (12.4) R_{\odot} at minimum (maximum). The highest measured height was 18.5 R_{\odot} . The histograms of these heights for the two LASCO intervals are shown in Figure 8b. For completeness the “ray length” results from Paper 1 have been included in Table 2. Although the SMM ray lengths are similar to LASCO, those were indirect measurements based on outward extrapolation of the C-O core assuming constant speed beyond the C/P FoV of 6 R_{\odot} .

3.5. Kinematics and Widths of the CME-Rays and Their Core Structures

For model comparisons it is of interest to measure and compare the kinematics and sizes of the CMEs with the rays and their associated C-O core structures. The width ratios of the main part of the CME to its core help us understand the size variation and geometry of the CMEs with rays, and the velocity ratios of the front (LE) of the CME to its core help measure the velocity dispersion and expansion of the CMEs with rays. Measurement of the height vs. time of the C-O edge allows us to track the kinematics of the growth of the CS. In each case we measured the back of each core feature, which is equivalent to the upper Y-point of the CS. Table 3 summarizes the statistical results of the velocities, accelerations, and widths of the CMEs with rays and their associated C-O cores for the two LASCO cycle intervals and the SMM period. The columns from left to right give 1) the time period, 2) the CME LE velocity, 3) the CME core velocity, 4) the ratio of the CME LE to core velocities,

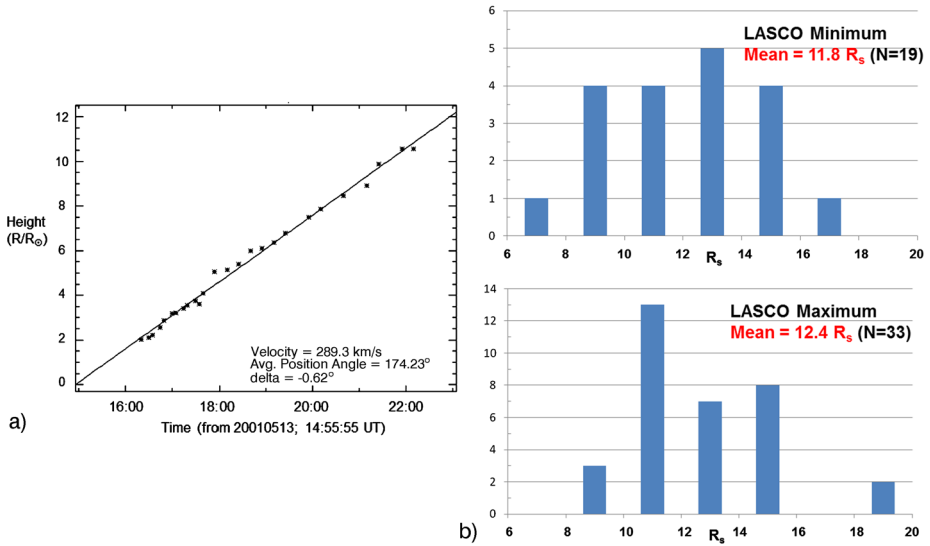


Figure 8 (a) Example of plot of height–time measurements of the trailing edge, or Y-point of the C-O feature through the C2 and C3 FoVs of a CME on 13 May 2001. The scatter of the points, especially in the C3 FoV above 4 R_{\odot} , is indicative of the accuracy of the measurements. The speed of this Y-point was 289 km s^{-1} , typical of those in 2001. (b) Histograms of these heights for the two LASCO intervals. The mean for both intervals was $\sim 12 R_{\odot}$ and the highest measured height was $18.5 R_{\odot}$.

Table 3 CMEs w/rays and CME core mean values: velocities, accelerations, and widths.

| 1 | 2 | 3 | 4 | 5 | 6 | 7 | 8 |
|--------------------------|---|----------------------------------|------------------------------|--|-----------------------------------|------------------------------|-----------------------------|
| Period (year) | LE vel. (km s^{-1}); CMEs w/rays | Core vel. (km s^{-1}) | LE/core velocity ratio | Core accel. (m s^{-2}) | Width ($^{\circ}$); CMEs w/rays | Width ($^{\circ}$); core | CME/core width ratio |
| 1996–Feb. 1998 | 434.1 ± 281.3 (42); 108–1556 | 187.9 ± 83.3 (27); 34–397 | 2.8 ± 3.0 (26); 0.6–17.0 | $+6.3 \pm 14.6$ (26); -6.4 to $+68.4$ | 67.7 ± 32.3 (44); 10–220 | 37.6 ± 20.7 (25); 13–87 | 1.9 ± 0.8 (25); 1.0–3.5 |
| 2001 | 715.8 ± 393.5 (85); 121–1750 | 324 ± 175.1 (40); 88–997 | 2.5 ± 1.25 (40); 0.8–6.0 | $+8.3 \pm 17.2$ (37); -45.2 to $+58.1$ | 70.8 ± 32.4 (65); 14–205 | 60.3 ± 31.1 (39); 14–134 | 1.6 ± 1.1 (33); 0.9–5.1 |
| SMM; 1984–1989 (Paper 1) | 218.5 (19); 16–577 | 130 (17); 35–417 | 1.6 ± 0.9 (12); 0.35–4.0 | N/A | 44 (23); 28–65 | 24 (25); 8–55 | 2.0 ± 1.2 (22); 0.7–5.4 |

5) the core acceleration, 6) the CME width, 7) the core width, and 8) the ratio of the main CME to core widths. In similar fashion to Table 2, each box gives the mean and standard deviation of each parameter, the number of measurements in parentheses, and the range of values. For example, in the second column and second row, “434.1” specifies the mean value in km s^{-1} of the velocity of the CME LE, “ ± 281.3 ” is the standard deviation of the mean, “(42)” is the total number of measurements made, and “108–1556” is the range in km s^{-1} of the velocities.

Referring to the velocities, as expected, the average velocities were lower at minimum than maximum. The SMM velocities (Paper 1) were considerably lower, possibly related

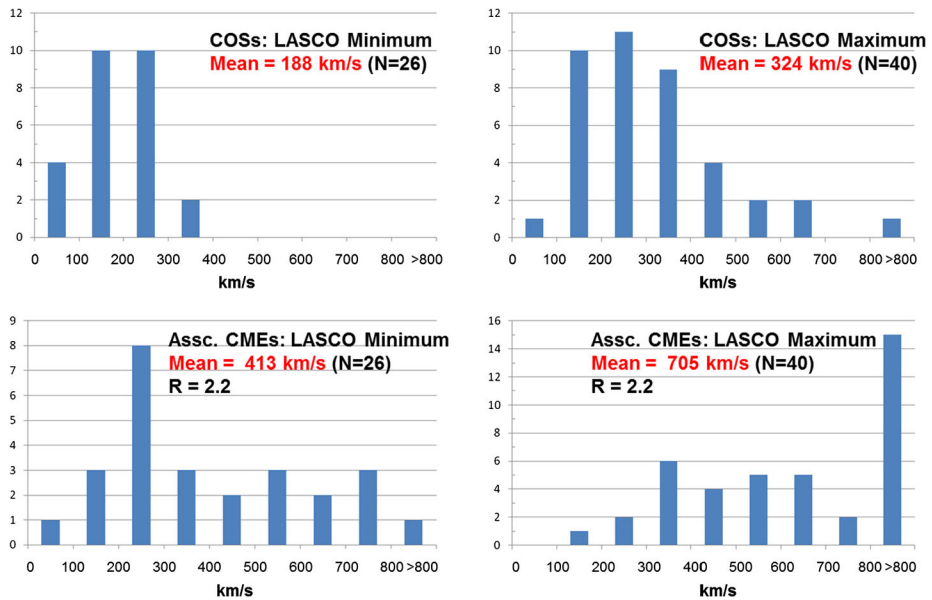


Figure 9 Histograms of the CME LE and their associated C-O core velocities, in 100 km s^{-1} bins, for the two LASCO intervals. As expected, the overall speeds were slower at cycle minimum than at maximum. The ratios of the CME front (LE) to back (core) speeds were 2.2 for both periods.

to the SMM C/P imaging quadrants, and they resulted in a lower cadence for viewing the full corona. The rate of height vs. time of the CME C-O structure associated with each ray provides the velocity of the increase in the CS length, or q in the model of Lin and Forbes. The mean as an estimate of the q velocity is 188 km s^{-1} (minimum) and 324 km s^{-1} (maximum), as shown in column 3 and in the top histograms of Figure 9. The SMM mean q was much lower. These q velocities are slower than the 416 km s^{-1} value found by Ling *et al.* (2014) for the fast September 2005 event. Its acceleration of 0.64 m s^{-2} was also much faster than our LASCO mean results, 6.3 and 8.3 m s^{-2} (Table 3, column 5).

The CME LE/core mean velocity ratios (column 4) were $2.5-2.8$, with not much difference between minimum and maximum. However, the SMM CME LE and core velocity ratio was much lower, 1.6 (but see next section). Histograms of the CME LE and core velocities for the two LASCO intervals are shown in Figure 9 (similar histograms for the SMM velocities are shown in the Appendix of Paper 1). The mean LASCO core accelerations were positive, with a large range (those for SMM were not recorded in Paper 1).

Columns 6–8 in Table 3 show results for the widths. We estimate that the width measurements are accurate to $\sim \pm 2^\circ$. The width distribution of the CMEs with rays (column 6) was similar for both minimum and maximum and to that of all CMEs (next section). At maximum, and for SMM, the CME cores were about a factor of two narrower and at maximum a factor of 1.6 narrower (column 8). The histograms of the CMEs with rays and their C-O core widths for the two LASCO intervals are shown in Figure 10 (similar histograms for the SMM widths are shown in the Appendix of Paper 1).

3.6. Comparison of Basic Parameters of CME-Rays with All CMEs

Again for model comparisons it is of interest to compare the basic parameters of the population of CME-rays to that of all CMEs to see if there are any significant differences that

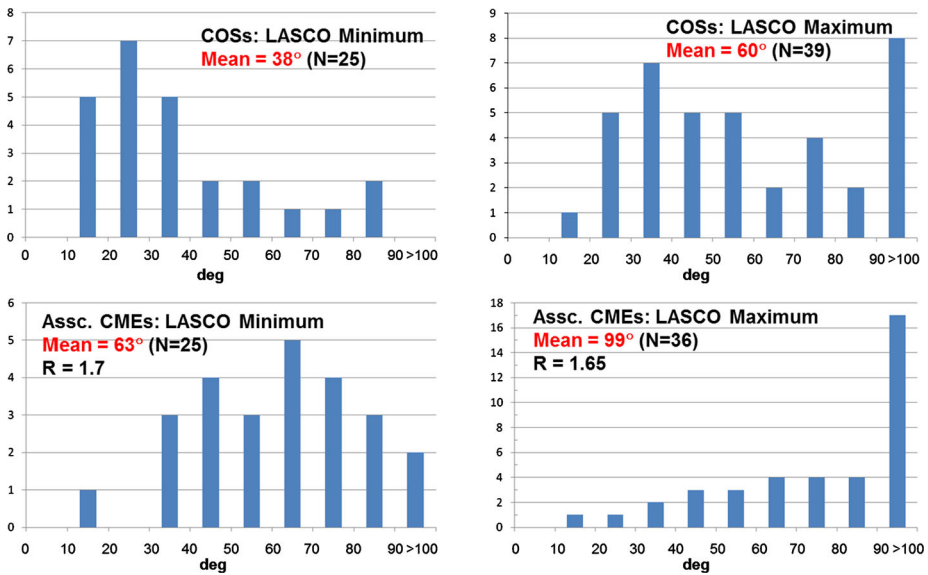


Figure 10 Histograms of the CMEs with rays and their associated C-O core widths, in 10° bins, for the two LASCO intervals. All of the mean widths were narrower at cycle minimum than maximum. The ratios of the CME front (LE) to back (core) widths were 1.7 for both periods.

Table 4 Basic parameters of CMEs.

| 1 | 2 | 3 | 4 | 5 | 6 | 7 | 8 | 9 |
|---------------------|--|--|------------------------|----------------------|--|--------------------------------------|--|--|
| Period (year) | LE vel. (km s ⁻¹); CMEs w/rays | LE vel. (km s ⁻¹); all CMEs* | Width (°); CMEs w/rays | Width (°); all CMEs* | Mass (10 ¹⁵ g); CMEs w/rays | Mass (10 ¹⁵ g); all CMEs* | Kinetic energy (10 ³⁰ erg); CMEs w/rays | Kinetic energy (10 ³⁰ erg); all CMEs* |
| 1996–Feb. | 434.1 ± | 322.5 ± | 67.7 ± 32.3 | 82 ± 43.9 | 3.0 ± 2.9 | 1.4 ± 1.4 | 4.5 ± 6.2 | 1.7 ± 2.3 |
| 1998 | 281.3 (42); 108–1556 | 130.2 (425); 39–1556 | (44); 10–220 | (425); 21–360 | (27); 0.02–10 | (425); 0.00–20 | (27); 0.01–20 | (425); 0.00–66 |
| 2001 | 715.8 ± | 471.3 ± | 70.8 ± 32.4 | 81.9 ± 47.1 | 2.65 ± 2.0 | 2.3 ± 2.3 | 5.1 ± 6.25 | 8.6 ± 1.3 |
| | 393.5 (85); 121–1750 | 214.2 (1184); 27–2505 | (65); 14–205 | (1184); 21–360 | (54); 0.15–7.3 | (1184); 0.01–97 | (53); 0.00–26 | (1184); 0.00–647 |
| SMM; | 218.5 (19); | 349 ± 289 | 44 (23); | 47 | N/A | N/A | N/A | N/A |
| 1984–1989 (Paper 1) | 16–577 | (936)** | 28–65 | (1209)** | | | | |

* Includes all CMEs >20° width, with measured masses and >3 measurements (Vourlidas *et al.*, 2010, 2013). The lowest ranges are very small and round off to 0.00.

** SMM CME velocities are from Hundhausen, Burkepile, and St. Cyr (1994) and widths from Hundhausen (1993).

might elucidate the eruptive CS process. Table 4 lists the statistical results of this comparison during the two LASCO cycle intervals and the SMM period. The basic parameters we examined are the CME LE velocity (columns 2–3), width (columns 4–5), mass (columns 6–7), and kinetic energy (columns 8–9). The results for all LASCO CMEs with widths

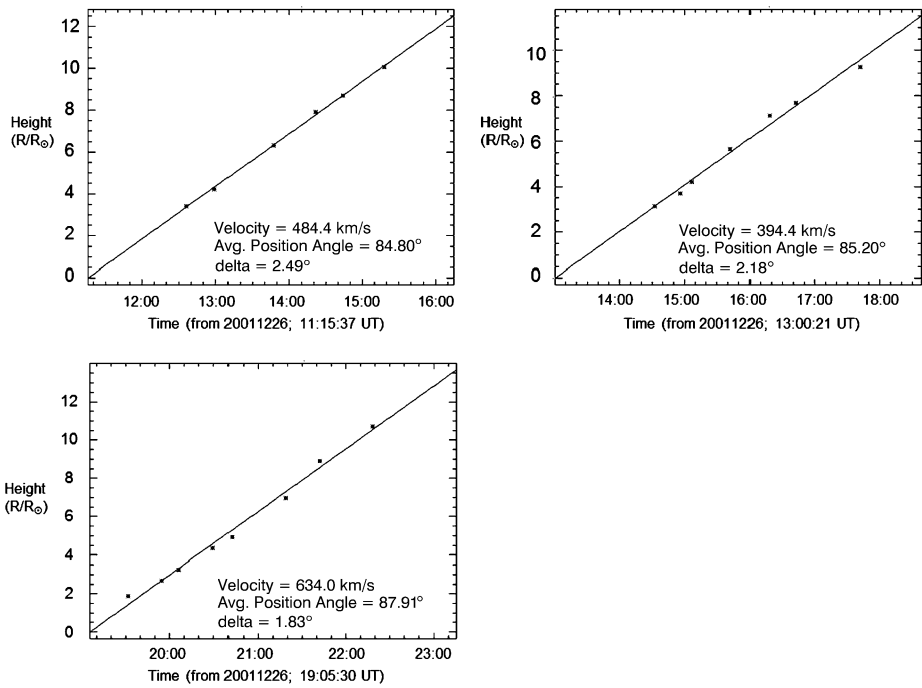


Figure 11 C2 + C3 height–time plots of three blobs that moved consecutively through a single CME-ray on 26 December 2001. Their speeds were 484, 394, and 634 km s⁻¹, respectively.

>20° are from the CDAW catalog, and for all SMM CME velocities and widths are from Hundhausen, Burkepile, and St. Cyr (1994) and Hundhausen (1993), respectively.

For the LASCO sample, the means of the velocities, masses, and kinetic energies of the CMEs with rays were either higher than or comparable to those of all LASCO CMEs. *Thus, these CMEs are not intrinsically different from the full population.* The mean SMM CME-ray velocities were much lower than both all SMM CMEs and either of the LASCO samples. The SMM CME-ray widths were only slightly lower than those of typical SMM CMEs. However, since the LASCO sample includes large populations of both narrow and wide CMEs that would probably not have been detected by SMM, it is difficult to make meaningful comparisons between the two distributions.

3.7. Velocities of Blobs; Evidence of Reconnection Outflows

Eruptive flare models imply that reconnection plasma outflows should appear moving along the current sheet away from the diffusion region in opposite directions (e.g., Bárta *et al.*, 2011; Shen, Lin, and Murphy, 2011; Mei *et al.*, 2012). Anti-sunward outflows observed in WL include coherent “blobs” propagating through the ray. Some of the rays in our study exhibited outflows and blobs, and we were able to make height–time measurements for 23 of them, or 18 % of the total sample.

Figure 11 shows the height–time plots of three consecutive blobs that moved through one ray. Their speeds ranged from 394–634 km s⁻¹ with accelerations from -3.1 to +33.9 ms⁻². The means, standard deviations, and ranges of our measurements of all of the LASCO blobs during the two intervals are given in Table 5. The blob velocities and

Table 5 Blob parameter means: velocities and accelerations.

| 1 | 2 | 3 |
|-----------------------------------|---------------------------------|-------------------------------------|
| Period (year) | Blob vel. (km s ⁻¹) | Blob accel. (m s ⁻²) |
| 1996–Feb. 1998 | 335.8 ± 84.3(6); 245–462 | +13.7 ± 0.5(3); +13.1 to +14.3 |
| 2001 | 377.5 ± 117.0(17); 201–634 | +17.7 ± 27.2(15); –38.1 to +63.6 |
| Song <i>et al.</i> ; 1999–2003 | 203–845 | –26.1 to +59.4 |

Table 6 Pre-existing streamers, blowouts, new streamers, and durations.

| 1 | 2 | 3 | 4 | 5 | 6 |
|--------------------------------|-------------------------|------------------------|--------------------------|-----------------------------|------------|
| Period (year) | P-E streamer? | Streamer blowouts | New streamer? | Duration: CME-new str. (hr) | Range (hr) |
| 1996–Feb. 1998 | 33Y, 11N, 3 CNT (47) | 25 (76 % of streamers) | 14Y, 16N, 13 CNT (43) | 28.5 (12) | 15–48 |
| 2001 | 34Y, 38N, 2 CNT (74) | 26 (76 % of streamers) | 17Y, 18N, 38 CNT (73) | 18.9 (13) | 5.5–28 |
| SMM; 1984–1989 (Paper 1) | 20Y, 1N, 5 CNT (26) | 14 (70 % of streamers) | 9Y, 7N, 2 CNT (18) | N/A | N/A |

accelerations were slightly higher during maximum than minimum, reflecting the increased speeds of the CMEs with rays and their C-O cores at maximum.

3.8. CME-Streamer Characteristics

For the transient rays, it is important to determine whether a new streamer has formed at the base of the ray after the CME has passed. As originally pointed out by Kahler and Hundhausen (1992), the appearance and growth of a new streamer, especially with a ray emanating outward from it, is indicative of reconnection in a CS and the subsequent closing of the loops below it to form an arcade. Thus, such observations lend support to CME reconnection models requiring CSs (*e.g.*, Lin and Forbes, 2000).

The example event shown in Figure 5 illustrates the pre-existing streamer, its blowout as the CME, and, in the last panel (e), the streamer reforming ~19 hr after CME onset. Table 6 shows the statistics on pre-existing streamers, blowouts, new streamers and durations compiled during this study. In column 2 we list whether the CME-ray arose from a pre-existing (P-E) streamer, in column 3 whether that streamer was blown out, and in column 4 whether we thought a new streamer appeared that was associated with the prior CME. An association was assumed if the new streamer was approximately (visually) coaligned with the axis of the CME and/or core, if it appeared within ~2 days of CME onset, and if it appeared to be growing with time. For the subset with new or reforming streamers, columns 5 and 6 list the mean duration and range, respectively, from the CME onset to the new streamer appearance time. This can be considered as the streamer reformation time.

To summarize the results of Table 6, there was a pre-existing streamer in 70 % (33 of 47) of the CME-ray events at minimum, and 46 % (34 of 74) during maximum. In about half

of these streamer events a new streamer developed after the CME-ray. In many of the cases we could not tell ('CNT') whether a new streamer developed, especially during maximum when coronal activity was greatest. The mean duration, or time to streamer reformation, was ~ 1 day after CME onset. This mean was higher (28.5 hr) at minimum than maximum (18.9 hr). In most (76 %) of the CME-ray events with pre-existing streamers the streamers were partially or completely blown out. These results for SMM CME-rays are shown in the last row of Table 6 and were similar (the streamer reformation time was not determined for SMM data).

4. Discussion

Current sheets are key structures of magnetic reconnection during flare and CME eruptions, and eruptive models involve the formation of a CS connecting the ejecting CME flux rope with a surface loop arcade. CSs have been associated in WL images with bright thin coaxial rays trailing the outward-moving CME. This study extends the Webb *et al.* (2003, Paper 1) and other studies of WL CMEs with trailing rays by providing the most comprehensive statistics of WL CME-ray properties: i) It uses SOHO/LASCO CME data, which have a higher cadence, increased FoV, and better sensitivity than SMM or any other previous coronagraph. ii) We examined *all* LASCO CMEs during two periods of minimum and maximum activity in Solar Cycle 23, resulting in many more events identified than during SMM (Paper 1). iii) The WL rays were observed and measured farther out than ever before – the C3 FoV extends to $32 R_{\odot}$, whereas the SMM FoV went to only $6 R_{\odot}$. iv) We made speed measurements for the largest sample to date of outflowing blobs within rays.

We studied a total of ~ 130 CME-rays and determined a variety of statistical results. These results include their occurrence rates, alignments and motions, durations or lifetimes, lengths, kinematics and widths, comparison of the basic parameters of the CMEs with rays *vs.* all CMEs, outflow or blob motions, and CME-streamer characteristics.

One aspect of the observations, which as far as we know no model can account for, is the relatively sudden appearance, or brightening, of a ray several hours after its apparent formation (mean of 3–4 hours). In such cases the ray brightens along its entire length, not just locally. The brightening itself is not well understood. It could be due to such factors as an increase in the emission measure, or density of the CS, an increase in the thickness of the sheet along the line of sight, or a change in the width orthogonal to the line of sight. In WL, the amount of dense plasma along the line of sight, the presence of background material, and the distance of the material from the plane of the sky all contribute to the detectability of coronal structures. Since present-day models lack physically realistic modeling of the reconnection process occurring in the current sheet, it could be that the brightening is related to a change in the reconnection rate after several hours. For example, if the reconnection rate were suddenly to decrease, then according to the Sweet–Parker theory (Parker, 1957) the sheet thickness should increase. The orientation of the CS could also evolve during the reconnection period, for example by rotating back and forth as a result of the release of twist and writhe in the erupting magnetic configuration. If the core structures of CMEs are interpreted as erupting flux ropes with trailing CSs, the detectability of the CS as a bright ray will depend on the density in the sheet as functions of time and height, and the orientation of the plane of the sheet with regard to the viewing angle (*e.g.*, Forbes and Acton, 1996). In addition, there is evidence that arcade brightenings can propagate with time from one end of the arcade to the other in a zipper-like fashion (*e.g.*, McAllister *et al.*, 1996; Qiu, 2015). This linear propagation of the arcade, as well as the related expansion of its footpoints, can be

a slow process, occurring over hours. Since the CS should magnetically connect the arcade to the flux rope, these brightenings could be related to reconnection in the CS and, hence, might appear as a delayed brightening of the WL ray.

Temperature effects are also possible. Coronagraphs are sensitive to only (electron) density along the line of sight. The UVCS-LASCO ray study of Ciaravella *et al.* (2013) demonstrated that hot material can be present where a CS is expected, even in the absence of a WL ray. The 23 March 1998 CME discussed by Ciaravella *et al.* (2002) is perhaps the best case of a CS apparently detected by UVCS as a narrow, dense, and hot feature but lacking a corresponding LASCO WL ray. Conversely, most of the WL rays did not exhibit [Fe XVIII] emission. For these events other UVCS lines indicated ray temperatures similar to the surrounding corona or cooler. It is also possible that the [Fe XVIII] emission was too weak to be detected. These observations show that both the density and temperature structure of CME-CSs are important in determining their detection in the corona, as well as the CS orientation.

A unique feature of the LASCO observations is that coronal structures can be observed as far out as the outer edge, $32 R_{\odot}$, of the C3 FoV. Use of the height–time measurements of the back of the CME core provides a new way of directly measuring the length of CME CSs in WL. The mean of all the “final” core heights measured in the C3 FoV is 11.8 (12.4) R_{\odot} at minimum (maximum). The highest measured height was $18.5 R_{\odot}$. The LASCO ray lifetimes were much longer than the SMM mean of 7.8 hr. The LASCO values are considered to be more reliable than those of SMM due to LASCO’s improved sensitivity, data cadence, and reduced stray-light level (see St. Cyr *et al.*, 2000 for a detailed comparison of the detectors).

In terms of the model of Lin and Forbes (2000), these C3 heights measure the distance, q , from the surface to the base of the flux rope. Ideally we need to know the length of the current sheet, $q - p$ (see Figure 3), but any associated surface arcade is never visible above the typical height of a coronagraph’s occulting disk (*e.g.*, $> 1.6 R_{\odot}$) at least during the ray lifetime. The arcade measured by Ling *et al.* (2014) with the low coronal MLSO data never rose higher than $0.3 R_{\odot}$ above the limb. These measured q heights are conservative underestimates. The base of the CME core can often be tracked by eye through the entire C3 FoV, but its faintness and broadening preclude reasonable measurement.

Paper 1 found that ~ 10 % of all the SMM CMEs had C-O cores. However, this rate varied over the solar cycle from about 8 % to 20 % with a tendency for such structures to be more common during solar minimum in 1984–1986. This suggested that they might be more visible at that epoch due to the simpler nature of the background coronal structure. However, using the more sensitive SOHO/LASCO coronagraphs, St. Cyr *et al.* (2000) found that on average 36 %, and possibly as high as 48 %, of LASCO CMEs exhibited C-O cores. This result was based on St. Cyr’s LASCO CME catalog discussed above, covering the period from 1996 through the end of June 1998. In a separate study covering about the same period, Dere *et al.* (1999) estimated that 25–50 % of LASCO CMEs had C-O circular structures that they interpreted as magnetic flux ropes. More recently, in a comprehensive examination of LASCO CMEs over SC 23, Vourlidas *et al.* (2013) found that at least 38 % of all CMEs had a flux-rope morphology.

The mean widths of the CMEs with rays, the CME C-O cores, and all CMEs were all considerably smaller for SMM than for LASCO, which might be due in part to the increased sensitivity of LASCO. These results for the large LASCO CME and core sample, however, confirm those of SMM (Paper 1) and Webb and Cliver (1995) that the cores are significantly narrower and slower than their accompanying CMEs.

We note that the increased sensitivity, FoV, and data cadence of LASCO leads to a higher occurrence rate of CME-rays (~ 11 %) compared to the SMM sample (~ 7 %) at solar

minimum. This increase seems consistent with the rate of detection of CMEs having a C-O morphology increasing from 10 % of all SMM CMEs to one-third to half of all LASCO CMEs. On the other hand, the fraction of observed C-O CMEs *with rays* decreased from more than half for SMM to only one-fifth for LASCO.¹ Thus, it appears that LASCO is more sensitive to the fainter and finer-scale CME structure and, hence, observes more C-O events, but why does it not see more rays? It is possible that the detectability of a ray in WL is extremely sensitive to the sheet orientation along the line of sight, which in turn suggests that CSs may be very narrow. Also, the larger number of CMEs during solar maximum likely obscures the ray signatures. If flux ropes typically form or are ejected in loss-of-equilibrium model scenarios, then the rate of circular CME structures observed by LASCO is probably closer to a true CS rate.

Eruptive flare models imply that reconnection plasma outflows should appear moving along the CS away from the diffusion region in opposite directions. As discussed in the Introduction, sunward flows have been well observed in association with the formation of the flare arcade loops. Anti-sunward outflows are associated with the evolution of the CME and flux rope structures, and are best observed in WL observations higher in the corona. As noted earlier, the outflows observed in WL within rays include coherent blobs propagating through the ray that might result from the tearing mode instability and lead to reconnecting islands in a CS. Some of the rays in our study exhibited outflows and blobs, and we were able to make height–time measurements for 23 of them.

A recent summary of the observations of reconnection outflows and some laboratory and numerical simulations are discussed by Lin *et al.* (2015). In general, the measured blob velocities and accelerations in our study are comparable to those of other studies. Ko *et al.* (2003) was probably the first to quantitatively measure outflow blobs in a bright, long-lived CS-ray observed in WL and EUV. UVCS measurements in the CS suggested temperatures of $3\text{--}6 \times 10^6$ K. The outflow speeds of 10 blobs ranged from 300 to 650 km s^{-1} , most with constant speed. Estimates of electron densities in two blobs in LASCO C2 at $3\text{--}4 R_{\odot}$ were $3\text{--}4 \times 10^6 \text{ cm}^{-3}$. Lin *et al.* (2005) found speeds of outward-moving blobs along the well-defined ray or CS in the event of 18 November 2003 of between 460 and 1075 km s^{-1} . This was suggestive of bursty reconnection in the current sheet, as modeled with magnetohydrodynamics (MHD) by, *e.g.*, Riley *et al.* (2007), Bárta *et al.* (2011), Shen, Lin, and Murphy (2011), and Mei *et al.* (2012). Recently, Song *et al.* (2012) investigated plasma blobs flowing inside 11 post-CME ray–CSs using LASCO data from 1996–2009, finding speeds over a large range from $\sim 200\text{--}845 \text{ km s}^{-1}$. A small majority of the blobs showed acceleration. Savage *et al.* (2010) and Takasao *et al.* (2012) measured CS blob outflows lower in the corona with *Hinode* XRT and LASCO observations on 9 April 2008, and SDO AIA observations on 18 August 2010, respectively. These two events exhibited both inward and outward flows. Savage *et al.* (2010) measured outflow velocities of $< 200 \text{ km s}^{-1}$, whereas Takasao *et al.* (2012) found a range of $220\text{--}460 \text{ km s}^{-1}$. They also observed merging of some blobs in the supposed CS. Merging of blobs in the CS was also shown in the numerical experiments by Bárta *et al.* (2011), Shen, Lin, and Murphy (2011), and Mei *et al.* (2012).

The study most similar to ours is that of Song *et al.* (2012), and their range of blob velocities and accelerations were very similar to ours (see last row of Table 5). Two of their

¹Since St. Cyr's LASCO CME catalog lists C-O features, we can check how many of those CME C-O events had rays that we identified. If we only take those CMEs with definite C-O structures, then during solar minimum 22 % (42 of 193) of the C-O CMEs had rays. A similar check for the 2001 maximum year could not be made because St. Cyr's catalog stopped after June 1998 and the CDAW catalog does not list C-O features.

ray events with blobs were also measured in our study, numbers 4 and 5 in 2001 in their Tables 1 and 2. For these rays they measured three and five blobs, respectively, whereas we only tracked one and two blobs. Despite this, the velocities of the two sets are similar. The single acceleration we measured for event 4, 11.9 m s^{-2} , is in the middle of their range, but our two values for event 5, 43 and 58 m s^{-2} , are well above their range of accelerations. We also estimated longer ray durations than Song *et al.* for the two events.

Unlike in the previous Paper 1 study, we did not attempt any width measurements of the LASCO CME-rays. This is because CME-ray widths in the corona are now well constrained through a variety of studies. Recent summaries of these coronal widths have been discussed by, *e.g.*, Ling *et al.* (2014) and Lin *et al.* (2015). It must be emphasized that we probably do not observe the CS itself in WL or other coronal wavelengths, but rather the plasma sheet surrounding it. This plasma sheet could arise, for example, from compression from the plasma inflowing into the reconnection region, and/or by the compression due to the expansion of the (now open) field above the X-point. In this sense the CS is like the stalk of a streamer. These measurements also usually assume projection on the plane of the sky. As discussed by Lin *et al.* (2015), traditional theory suggests a CS is as thin as the proton Larmor radius, which is on the order of tens of meters in the corona. However, in actual dynamic coronal eruptions, plasma instabilities and turbulence should be important and could lead to broadening of CSs (*e.g.*, Lin *et al.*, 2007). In observational results (*e.g.*, Lin *et al.*, 2009), the thickness of the CS is calculated to be much larger than classical or anomalous resistivity would predict, possibly indicating an effective resistivity much higher than anomalous resistivity, such as that due to hyperdiffusion. The Petschek reconnection mechanism (Petschek, 1964) and turbulent reconnection may be consistent with these results. See Lin *et al.* (2015) for an extensive review of observations of CS thickness compared with theory and simulations. In addition, CSs observed at higher temperatures might be surrounded by a “thermal halo” (*e.g.*, Reeves *et al.*, 2010). All these effects suggest that the observed ray or CS widths tend to be upper limits to their true widths.

We note that eruptive flare models also predict a reconnection *inflow* near the CS, which is considered as another observational consequence of such models. This inflow motion brings magnetized plasma into the CS and is a function of the rate of energy conversion in the process. Thus, the rate of reconnection, M_A , is related to the velocity of the inflow compared to the local Alfvén speed near the CS. Yokoyama *et al.* (2001) first identified apparent reconnection inflow above the top of a flare loop system. Later, Lin *et al.* (2005) made direct measurements of the reconnection inflow speed near a CS, obtained the reconnection outflow speed of five moving plasma blobs, and the rate of reconnection. However, detecting and measuring this inflow in the corona remains difficult (*e.g.*, see Vršnak *et al.*, 2009), and an unambiguous observation of a CS X-point or diffusion region, at least in WL, has yet to be made. In our study we did not visually observe obvious inflows associated with the rays. Such an analysis remains for future work.

Finally, the authors are involved in a study of the 3D geometry of WL rays using both LASCO and SECCHI coronagraph data following the pioneering work of Patsourakos and Vourlidas (2011). This new study is providing an improved understanding of the geometry, kinematics, and plasma characteristics of WL rays or CSs. Kwon, Vourlidas, and Webb (2016) have published the first results: determining the 3D properties of a CME ray derived from WL images obtained from three different viewing perspectives. Using forward-modeling, the direction, cross section, and electron density were determined within the corona from $5\text{--}9 R_\odot$. Successive blobs moving outward along the ray were observed ~ 13 hours after the parent CME onset, and their kinematics were analyzed.

5. Conclusions

This work extends the study of CME-rays observed by SMM (*e.g.*, Webb *et al.*, 2003, Paper 1) to the more sensitive and extensive SOHO/LASCO coronagraph data on CMEs. LASCO CME-rays were analyzed during minimum and maximum activity periods of SC 23. The most important results of this study are listed below.

- The occurrence rate of the LASCO CME-rays or CSs is $\sim 11\%$ of all CMEs during minimum, dropping to $\sim 7\%$ at solar maximum. The former is likely a more accurate representation of the true rate due to the better observation conditions during solar minimum.
- The CME-rays appear an average of 3–4 hours after the CME core or C-O structure left the FoV.
- The CME-rays are typically visible for three-fourths of a day.
- The highest measured heights of the CME C-O structure associated with the rays were used to determine the CS length, or q in the model of Lin and Forbes (2000). The mean of q over the mean lifetime of three-fourths of a day is $\sim 12 R_{\odot}$. The highest measured value is $18.5 R_{\odot}$. The long lifetime and long lengths of the CME-rays are challenging for our current understanding of the evolution of the magnetic field in the aftermath of CMEs.
- The mean velocities of the increase in the CS length, or q , are 188 km s^{-1} at minimum and 324 km s^{-1} at maximum. The mean accelerations are 6.3 and 8.3 m s^{-2} .
- The kinematics of WL blobs observed through the rays provides evidence of reconnection outflows. Outward-moving blobs within several rays have average velocities of $\sim 350 \text{ km s}^{-1}$ with small positive accelerations. These values are consistent with previous results.
- A pre-existing streamer is blown out as the CME in three-fourths of the ray events. Half of these streamer blowouts are observed to re-form within an average of ~ 1 day. Since WL streamers form the base of the HCS, these results bear on the evolution of the basic heliospheric solar wind structure.

Acknowledgements This work was performed by D.F.W. at Boston College under NASA grants NNX09AB17G-R, NNX11AB61G, and NNX13AG54G. A.V. was supported by NNX13AV25I and internal APL funds. We are grateful to S. Yashiro and O.C. St. Cyr for data and helpful comments. The SOHO/LASCO data used here are produced by a consortium of the Naval Research Laboratory (USA), Max-Planck-Institut fuer Sonnensystemforschung (Germany), Laboratoire d'Astronomie (France), and the University of Birmingham (UK). SOHO is a project of international cooperation between ESA and NASA. We made extensive use of the SOHO/LASCO CDAW CME catalog, generated and maintained by the Center for Solar Physics and Space Weather, The Catholic University of America in cooperation with NRL and NASA. D.F.W. benefitted from a series of workshops on understanding the role of current sheets in solar eruptive phenomena at the International Space Sciences Institute (ISSI) in Bern, Switzerland.

Conflict of interest The authors declare that they have no conflicts of interest.

References

- Bárta, M., Büchner, J., Karlický, M., Kotrč, P.: 2011, *Astrophys. J.* **730**, 47. DOI.
- Brueckner, G.E., Howard, R.A., Koomen, M.J., Korendyke, C.M., Michels, D.J., Moses, J.D., *et al.*: 1995, *Solar Phys.* **162**, 357. DOI.
- Burkepile, J.T., St. Cyr, O.C.: 1993, A revised and expanded catalogue of mass ejections observed by the solar maximum mission coronagraph. Rep. NCAR/TN-369+STR, Natl. Cent. for Atmos. Res., Boulder, CO.

- Chen, P.F.: 2011, *Living Rev. Solar Phys.* **8**, 1. DOI.
- Chen, J., Howard, R.A., Brueckner, G.E., Santoro, R., Krall, J., Paswaters, S.E., St. Cyr, O.C., Schwenn, R., Lamy, P., Simnett, G.M.: 1997, *Astrophys. J.* **490**, L191. DOI.
- Ciaravella, A., Raymond, J.C., Li, J., Reiser, P., Gardner, L.D., Ko, Y.-K., Fineschi, S.: 2002, *Astrophys. J.* **575**, 1116. DOI.
- Ciaravella, A., Raymond, J.C., van Ballegooijen, A., Strachan, L., Vourlidas, A., Li, J., Chen, J., Panasyuk, A.: 2003, *Astrophys. J.* **597**, 1118. DOI.
- Ciaravella, A., Webb, D.F., Giordano, S., Raymond, J.C.: 2013, *Astrophys. J.* **766**, 65. DOI.
- DeForest, C.E., Howard, T.A., McComas, D.J.: 2012, *Astrophys. J.* **745**, 36. DOI.
- Dere, K.P., Brueckner, G.E., Howard, R.A., Michels, D.J., Delaboudiniere, J.P.: 1999, *Astrophys. J.* **516**, 465. DOI.
- Fisher, R.R., Lee, R.H., MacQueen, R.M., Poland, A.I.: 1981, *Appl. Opt.* **20**, 1094. DOI.
- Forbes, T.G., Acton, L.W.: 1996, *Astrophys. J.* **459**, 330. DOI.
- Giordano, S., Ciaravella, A., Raymond, J.C., Ko, Y.-K., Suleiman, R.: 2013, *J. Geophys. Res.* **118**, 967. DOI.
- Guo, L.-J., Bhattacharjee, A., Huang, Y.-M.: 2013, *Astrophys. J.* **771**, L14. DOI.
- Hundhausen, A.J.: 1993, *J. Geophys. Res.* **98**, 13177. DOI.
- Hundhausen, A.J., Burkepile, J.T., St. Cyr, O.C.: 1994, *J. Geophys. Res.* **99**, 6543. DOI.
- Kahler, S.W., Hundhausen, A.J.: 1992, *J. Geophys. Res.* **97**, 1619. DOI.
- Ko, Y., Raymond, J.C., Lin, J., Lawrence, G., Li, J., Fludra, A.: 2003, *Astrophys. J.* **594**, 1068. DOI.
- Kohl, J.L., Esser, R., Gardner, L.D., Habbal, S., Daigneau, P.S., Dennis, E.F., et al.: 1995, *Solar Phys.* **162**, 313. DOI.
- Kwon, Y., Vourlidas, A., Webb, D.: 2016, *Astrophys. J.* **826**, 94. DOI.
- Lin, J.: 2004, *Solar Phys.* **219**, 169. DOI.
- Lin, J., Forbes, T.G.: 2000, *J. Geophys. Res.* **105**, 2375. DOI.
- Lin, J., Raymond, J.C., van Ballegooijen, A.A.: 2004, *Astrophys. J.* **602**, 422. DOI.
- Lin, J., Ko, Y.-K., Sui, L., Raymond, J.C., Stenborg, G.A., Jiang, Y., Zhao, S., Mancuso, S.: 2005, *Astrophys. J.* **622**, 1251. DOI.
- Lin, J., Li, J., Forbes, T.G., Ko, Y.-K., Raymond, J.C., Vourlidas, A.: 2007, *Astrophys. J.* **658**, L123. DOI.
- Lin, J., Li, J., Ko, K., Raymond, J.C.: 2009, *Astrophys. J.* **693**, 1666. DOI.
- Lin, J., Murphy, N.A., Shen, C., Raymond, J.C., Reeves, K.K., Zhong, J., Wu, N., Li, Y.: 2015, *Space Sci. Rev.* **194**, 237. DOI.
- Ling, A.G., Webb, D.F., Burkepile, J.T., Cliver, E.W.: 2014, *Astrophys. J.* **784**, 91. DOI.
- Linker, J.A., Mikic, Z., Lionello, R., Riley, P., Amari, T., Odstrcil, D.: 2003, *Phys. Plasmas* **10**, 1971. DOI.
- MacQueen, R.M., Csoeke-Poeckh, A., Hildner, E., House, L., Reynolds, R., Stanger, A., Tepoel, H., Wagner, W.: 1980, *Solar Phys.* **65**, 91. DOI.
- McAllister, A.H., Dryer, M., McIntosh, P., Singer, H., Weiss, L.: 1996, *J. Geophys. Res.* **101**(A6), 13497. DOI.
- McComas, D.J., Gosling, J.T., Phillips, J.L.: 1992, *J. Geophys. Res.* **97**, 171. DOI.
- McComas, D.J., Gosling, J.T., Phillips, J.L., Bame, S.J., Luhmann, J.G., Smith, E.J.: 1989, *J. Geophys. Res.* **94**, 6907. DOI.
- Mei, Z., Shen, C., Wu, N., Lin, J., Murphy, N.A., Rousev, I.I.: 2012, *Mon. Not. Roy. Astron. Soc.* **425**, 2824. DOI.
- Parker, E.N.: 1957, *J. Geophys. Res.* **62**, 509. DOI.
- Patsourakos, S., Vourlidas, A.: 2011, *Astron. Astrophys.* **525**, A27. DOI.
- Patsourakos, S., Vourlidas, A., Stenborg, G.: 2010, *Astrophys. J.* **724**, L188. DOI.
- Petschek, H.E.: 1964, In: Hess, W.N. (ed.) *The Physics of Solar Flares SP-50*, NASA, Washington, 425.
- Qiu, J.: 2015, How the dynamics of flare ribbons can help us understand the three-dimensional structure of reconnection. In: *Triennial Earth–Sun Summit, TESS, Indianapolis, IN, 27–30 April, 2015*, Abs. 104.02.
- Reeves, K.K., Linker, J.A., Mikic, Z., Forbes, T.G.: 2010, *Astrophys. J.* **721**, 1547. DOI.
- Riley, P., Lionello, R., Mikic, Z., Linker, J., Clark, E., Lin, J., Ko, Y.-K.: 2007, *Astrophys. J.* **655**, 591. DOI.
- Savage, S.L., McKenzie, D.E., Reeves, K.K., Forbes, T.G., Longcope, D.W.: 2010, *Astrophys. J.* **722**, 329. DOI.
- Sheeley, N.R., Wang, Y.-M.: 2007, *Astrophys. J.* **655**, 1142. DOI.
- Shen, C., Lin, J., Murphy, N.A.: 2011, *Astrophys. J.* **737**, 14. DOI.
- Shibata, K., Masuda, S., Shimojo, M., Hara, H., Yokoyama, T., Tsuneta, S., Kosugi, T., Ogawara, Y.: 1995, *Astrophys. J.* **451**, L83. DOI.
- Simnett, G.M.: 2004, *Astron. Astrophys.* **416**, 759. DOI.
- Simnett, G.M., Tappin, S.J., Plunkett, S.P., Bedford, D.K., Eyles, C.J., St. Cyr, O.C., et al.: 1997, *Solar Phys.* **175**, 685. DOI.
- Song, H., Kong, X., Chen, Y., Li, B., Li, G., Feng, S., Xia, L.: 2012, *Solar Phys.* **276**, 261. DOI.

- St. Cyr, O.C., Howard, R.A., Sheeley, N.R. Jr., Plunkett, S.P., Michels, D.J., Paswaters, S.E., *et al.*: 2000, *J. Geophys. Res.* **105**, 18169. [DOI](#).
- Svestka, Z., Cliver, E.W.: 1992, In: Svestka, Z., Jackson, B., Machado, M. (eds.) *Eruptive Solar Flares, History and Basic Characteristics of Eruptive Flares*, Springer, New York, 1.
- Takasao, S., Asai, A., Isobe, H., Shibata, K.: 2012, *Astrophys. J.* **745**, L6. [DOI](#).
- Vourlidas, A., Howard, R.A., Esfandiari, E., Patsourakos, S., Yashiro, S., Michalek, G.: 2010, *Astrophys. J.* **722**, 1522. [DOI](#).
- Vourlidas, A., Howard, R.A., Esfandiari, E., Patsourakos, S., Yashiro, S., Michalek, G.: 2011, ERRATUM: "Comprehensive analysis of coronal mass ejection mass and energy properties over a full solar cycle" (2010, *Astrophys. J.*, **722**, 1522). *Astrophys. J.* **730**, 59. [DOI](#).
- Vourlidas, A., Lynch, B.J., Howard, R.A., Li, Y.: 2013, *Solar Phys.* **284**, 179. [DOI](#).
- Vršnak, B., Poletto, G., Vujić, E., Vourlidas, A., Ko, Y.-K., Raymond, J.C., *et al.*: 2009, *Astron. Astrophys.* **499**, 905. [DOI](#).
- Wang, Y.-M., Colaninno, R.: 2014, *Astrophys. J.* **784**, L27. [DOI](#).
- Wang, Y.-M., Sheeley, N.R. Jr., Howard, R.A., Rich, N.B., Lamy, P.L.: 1999, *Geophys. Res. Lett.* **26**, 1349. [DOI](#).
- Webb, D.F., Cliver, E.W.: 1995, *J. Geophys. Res.* **100**, 5853. [DOI](#).
- Webb, D.F., Burkepile, J., Forbes, T.G., Riley, P.: 2003, *J. Geophys. Res.* **108**(A12), 1. [DOI](#) (Paper 1).
- Yashiro, S., Gopalswamy, N., Michalek, G., St. Cyr, O.C., Plunkett, S.P., Rich, N.B., Howard, R.A.: 2004, *J. Geophys. Res.* **109**, A07105. [DOI](#).
- Yokoyama, T., Akita, K., Morimoto, T., Inoue, K., Newmark, J.: 2001, *Astrophys. J.* **546**, L69. [DOI](#).